

Water Resources Research

RESEARCH ARTICLE

10.1029/2020WR028478

Using Additional Moderator to Control the Footprint of a COSMOS Rover for Soil Moisture Measurement



Key Points:

- The possibility of using high density polyethylene moderator on a set of Cosmic-Ray Neutron Probes (Rovers) to limit the field of view is explored
- Neutron scattering simulations show that the moderator provides considerable control over the sensor's footprint
- The Rover was used to conduct measurements on a stubble field to test the system in measuring spatial and temporal soil moisture variation

Amir Badiee^{1,9} , John R. Wallbank², Jaime Pulido Fentanes³, Emily Trill² , Peter Scarlet², Yongchao Zhu^{4,5}, Grzegorz Cielniak⁹ , Hollie Cooper² , James R. Blake² , Jonathan G. Evans² , Marek Zreda⁶, Markus Köhli^{7,8} , and Simon Pearson⁹ 

¹Engineering School, The University of Lincoln, Lincoln, UK, ²UK Centre for Ecology & Hydrology (UKCEH), Wallingford, UK, ³Saga Robotics, Ruston Way, UK, ⁴State Key Laboratory of Severe Weather, Chinese Academy of Meteorological Sciences, Beijing, China, ⁵Collaborative Innovation Center on Forecast and Evaluation of Meteorological Disasters, Nanjing University of Information Science and Technology, Nanjing, China, ⁶Hydrology and Atmospheric Sciences Department, University of Arizona, Tucson, AZ, USA, ⁷Physikalisches Institut, Heidelberg University, Heidelberg, Germany, ⁸Physikalisches Institut, University of Bonn, Bonn, Germany, ⁹Lincoln Institute for Agri-Food Technology (LIAT), The University of Lincoln, Lincoln, UK

Correspondence to:

A. Badiee and J. G. Evans,
abadiee@lincoln.ac.uk;
jge@ceh.ac.uk

Citation:

Badiee, A., Wallbank, J. R., Fentanes, J. P., Trill, E., Scarlet, P., Zhu, Y., et al. (2021). Using additional moderator to control the footprint of a COSMOS Rover for soil moisture measurement. *Water Resources Research*, 57, e2020WR028478. <https://doi.org/10.1029/2020WR028478>

Received 27 JUL 2020

Accepted 18 MAY 2021

Abstract Cosmic-Ray Neutron Probes (CRNP) have found application in soil moisture (SM) estimation due to their conveniently large (>100 m) footprints. Here, we explore the possibility of using high-density polyethylene (HDPE) moderator to limit the field of view, and hence, the footprint of a SM sensor formed of 12 CRNP mounted on to a mobile robotic platform (Thorvald) for better in-field localization of moisture variation. Ultra Rapid Adaptable Neutron-Only Simulation neutron scattering simulations are used to show that 5 cm of additional HDPE moderator (used to shield the upper surface and sides of the detector) is sufficient to (a) reduce the footprint of the detector considerably, (b) approximately double the percentage of neutrons detected from within 5 m of the detector, and (c) does not affect the shape of the curve used to convert neutron counts into SM. Simulation and rover measurements for a transect crossing between grass and concrete additionally suggest that (d) SM changes can be sensed over a length scales of tens of meters or less (roughly an order of magnitude smaller than commonly used footprint distances), and (e) the additional moderator does not reduce the detected neutron count rate (and hence increase noise) as much as might be expected given the extent of the additional moderator. The detector with additional HDPE moderator was also used to conduct measurements on a stubble field over three weeks to test the rover system in measuring spatial and temporal SM variation.

1. Introduction

Soil Moisture (SM) is a crucial variable in hydrological cycles and affects weather prediction, climate studies, greenhouse gas control, hydrological modeling, weather prediction, climate forecasts, modeling of greenhouse gas exchanges, and ecosystem monitoring. In addition, measuring SM offers the opportunity to adapt and optimize agricultural strategies, including irrigation and risk mitigation, that reduce the impacts of climate variability on crop and plant growth (Beljaars et al., 1996; Dirmeyer, 1999; Entekhabi & Rodriguez-Iturbe, 1994; Entin et al., 2000; Koster, 2004; Wang et al., 2006).

One of the most commonly used SM measurement techniques is point measurement (e.g., time domain reflectometry [TDR]; Robinson et al., 2003, 2008). However, due to the spatial heterogeneity of SM, point-based techniques lack representativeness (Entin et al., 2000; Famiglietti et al., 1999; Western & Blöschl, 1999). Accurate measurements require high replication in both time and space which is expensive and practically challenging (Bogena et al., 2010; Famiglietti et al., 1999; Famiglietti et al., 2008; Western et al., 2002). More recently radar-based techniques, typically using satellite data, have been explored for estimating SM at the landscape scale. This method is limited by shallow penetration depths (Entekhabi et al., 2004; Njoku & Entekhabi, 1996), challenging signal analysis not least due to local variances in vegetation and surface roughness (Robinson et al., 2008), discontinuous temporal coverage, high cost and relative short life spans of satellite missions (Al-Yaari et al., 2014).

© 2021. The Authors.

This is an open access article under the terms of the [Creative Commons Attribution License](https://creativecommons.org/licenses/by/4.0/), which permits use, distribution and reproduction in any medium, provided the original work is properly cited.

More recent approaches have tended to focus on ground sensors that have medium range sensing capability (hundreds of meters), sensing at depth and with high precision, including distributed temperature sensing (Steele-Dunne et al., 2010), use of global positioning system signals (Larson et al., 2008) or wireless sensor networks (Bogena et al., 2010). However, the technology which has received interest in the recent years, employs Cosmic-Ray Neutron Sensing (CRNS; Zreda et al., 2008) to estimate SM using the fact that the intensity of cosmic ray generated neutrons is inversely correlated with the amount of water present in the surrounding environment. CRNS is a non-invasive, non-contact technique suitable for long-term soil monitoring. Initially, Kodama et al. (1985) measured SM using cosmic neutrons by placing detectors in the soil, giving a highly localized measurement (order of decimeters). Mounting neutron detectors above the soil surface enabled a much larger CRNS measurement area (also known as the footprint) with a radius of hundreds of meters (Desilets & Zreda, 2013; Köhli et al., 2015), a field of view suitable for land surface modeling and agricultural applications (Baatz et al., 2015; Finkenbinder et al., 2019; Han et al., 2015; Iwema et al., 2017; Ochsner et al., 2013). Since its introduction, CRNS technology has quickly established itself for hydrological observations (Andreasen et al., 2017) and is now used for SM monitoring worldwide (Bogena et al., 2013; Franz et al., 2013; Peterson et al., 2016; Schrön et al., 2018; Zhu et al., 2016). Large networks of cosmic-ray probes, have been deployed and distributed mainly in the USA (<http://cosmos.hwr.arizona.edu>) and approximately 50 probes have been deployed across the UK (COSMOS-UK network; Evans et al., 2017; Zreda et al., 2012).

Cosmic-Ray Neutron Probes (CRNP) are typically deployed as static probes, but more recently they have also been explored as mobile probes attached to ground based vehicles (Avery et al., 2018; Avery, 2016; Chrisman & Zreda, 2013; Desilets et al., 2010; Dong et al., 2014; McJannet et al., 2014, 2017; Schrön et al., 2018). This approach enables CRNP deployment to measure spatial variance of SM. For example, Franz et al. (Franz et al., 2015, 2016) investigated the suitability of the CRNS method for real-time SM monitoring by combining fixed probes and roving techniques over a large area at a spatial resolution of 1 km to fill the gap between point sensors and remote sensing products. These studies suggested the potential of mobile CRNP as a stand-off methodology for measuring spatial SM variance.

One factor which can influence the neutron count is the presence of vegetation. Various studies (Baatz et al., 2015; Baroni & Oswald, 2015; Franz et al., 2013, 2015; Hawdon et al., 2014; Hornbuckle et al., 2012; Jakobi et al., 2018; Tian et al., 2016) investigated such impact which might require the correction for site biomass, to account for the attenuation of the cosmic ray neutron intensity by biomass, and to improve the accuracy of the CRNS's soil water content estimates. Other studies (Andreasen et al., 2017; Bogena et al., 2013; Vather et al., 2020) showed that hydrogen present in the biomass can decrease the neutron intensity and the overall accuracy of the CRNS especially in humid forests with high vegetation's such as trees.

High resolution spatial SM has considerable application value especially in agricultural systems, where understanding the effects of SM on crop growth or to optimize machinery/irrigation use is critical. However, for accurate measurement mobile CRNP devices require multiple CRNP stacked together (rover). Multiple probes reduce the statistical error by increasing the neutron count rate (Jakobi et al., 2020).

Previous studies found that the shape of the footprint is limiting the applicability of the standard CRNS instrument for large-scale SM mapping due to the strong influence of local features such as dry roads (Schrön et al., 2018). Although the measurement of local features are relevant for irrigation management, it has been shown that this is not feasible with the standard large-scale CRNS instrument (Li et al., 2019). Ergo, this brought us to the idea of an instrument with limited footprint. This study demonstrates a novel mobile CRNP mounted on a robotic platform for easier in-field relocation of the sensors. We show and model how the instrument's footprint can be modified by the use of high-density polyethylene (HDPE) moderator. Accordingly, neutron scattering simulations were conducted and suitable measurement sites were selected to assess the footprint length scale of the rover with and without additional moderator, and to demonstrate how the rover could measure SM at high spatial and temporal resolution.

2. Methodology

2.1. Cosmic-Ray Neutrons and Soil Moisture Measurement

The principals of the CRNS technique is similar to the neutron probe developed by the Institute of Hydrology, Wallingford, UK (Institute of Hydrology, 1981); however, this technique uses naturally occurring neutrons generated by cosmic rays and does not require an artificial radioactive neutron source – greatly reducing safety and security concerns, allowing the CRNP to be continuously deployed in the field, unattended. The CRNS technique is based on the dependence of the epithermal cosmic neutron intensity (Motteff, 1970; Zreda et al., 2008) on the hydrogen content of soil. Theoretical work showed that the intensity of low-energy neutrons does not depend on the chemical composition but mainly on hydrogen content of the environment (Bethe et al., 1940; Zreda et al., 2008). The interaction between epithermal neutrons ($\gtrsim 0.5$ eV) with hydrogen is used for SM estimation (Köhli et al., 2015; Zreda et al., 2008). Low energy neutrons interact with hydrogen and therefore the neutron albedo is a proxy for SM as wet soil moderates neutrons more than dry soil (Bethe et al., 1940; Fermi et al., 1934; Zreda et al., 2012).

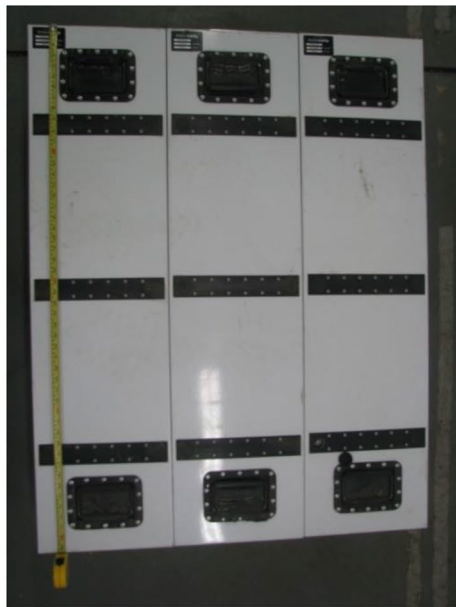
Zreda et al. (2008) demonstrated that placing a neutron detector above the ground allowed measurement of average SM over a horizontal area of hectometers and to a depth of decimeters. A footprint length (defined as the radius of the area from within which 86% of the detected neutrons have interacted with the soil) was found to be almost 300 m for dry air at sea level (Desilets & Zreda, 2013) and depended significantly on air humidity, or about 120–230 m (Köhli et al., 2015) and depended on both humidity and SM.

2.2. Cosmic-Ray Probe Measurement System

In this experiment, we combined a large array of neutron detectors (rover) with a robotic platform (Thorvald robot, Saga Robotics; Grimstad & From, 2017), see Figure 1. The robot has a mass of 180 kg and is powered by up to two 48 V Li-Ion batteries with 70 Ah capacity, giving a functional life of 10 h (Saga Robotics, 2020). The rover is highly maneuverable and enables autonomous sensing of large spatial areas across agricultural systems. The mobile CRNS detector array comprised 12 boron trifluoride neutron detectors (Hydroinnova LLC) stacked in three containers each called rover (serial numbers: HI-DM-1101, HI-DM-1102, HI-DM-1103); four per container each in a 2×2 layered array (Figures 1a and 1b). Total mass of the mobile sensor without additional moderator is 180 kg. CRNPs were connected to a portable data logger along with an air temperature and air humidity probe (model CS215, Campbell Scientific, Ltd). In addition, we conducted experiments to limit the field of view of the rover by adding an additional 5 cm of HDPE moderator on the top and sides (but not the bottom) of the three detector containers. This increased the detector mass to 380 kg (Figures 1b and 1c). To estimate SM content, the detected neutron counts were corrected for the incoming variation of cosmic rays (using counts from the Jungfraujoch neutron monitor), the air mass above the sensor (air pressure) and water vapor in the air to obtain corrected neutron count rate as presented in Appendix A (Hawdon et al., 2014; Rosolem et al., 2013; Schrön et al., 2015; Zreda et al., 2012).

2.3. Simulated Neutron Detectors (URANOS)

The neutron transport modeling was conducted using the Ultra Rapid Adaptable Neutron-Only Simulation (URANOS) Monte Carlo code (Köhli et al., 2015; version 0.99 ω 2 except where stated) with neutron cross-section files (v0.99+; both downloaded on 2019-08-08 and available from <https://www.physi.uni-heidelberg.de/Forschung/ANP/Cascade/URANOS/>). Briefly, neutrons are injected randomly within a source layer in the lower atmosphere with an energy spectrum designed to mimic incoming cosmic ray neutrons (Sato, 2016). They lose energy through random collisions in the atmosphere, soil, and moderator before either reaching thermal energies, or are detected by a neutron detector. Here the modeled atmosphere was 1,000 m deep, the source layer for neutron injection into the model was between heights of 50–80 m, and the soil depth was 1.6 m. The soil porosity was set at 50% with a bulk density of 1.43 g/cm^3 , the atmospheric humidity was 10 g/m^3 , and the cut-off rigidity was 10 GV. Out of these, only the atmospheric humidity is expected to have a significant effect on the detector's footprint (e.g., reducing humidity by 5 g/m^3 would increase the $R(e_2)$ -footprint by around 5%; Köhli et al., 2015).



(a)



(b)



(c)



(d)



(e)

Figure 1. (a) Twelve neutron detectors stacked 2×2 within three containers (each container is called rover with dimensions of L : 125 cm and W : 32 cm), (b) The detectors are shown in an open box where they are stacked 2×2 (Detectors 1 and 2 are shown), (c) The additional high-density polyethylene (HDPE) moderator on top and sides of the rovers (the open side is for demonstration). Three Rovers mounted on the robot (d) without, and (e) with additional HDPE moderator.

Single rectangular detectors with dimensions of $1 \times 1 \times 0.33$ m (width \times depth \times height) were used to simulate the assemblage of 12 moderated CRNP tubes forming the actual detector. These were set at a height of 0.86 m (to bottom of detector), and optionally had either 0, 5, or 10 cm of additional HDPE moderator on the top and sides. Except as stated below, each simulation employed 80 million neutrons, injected over a $1,000 \times 1,000$ m area and tracked regardless of their distance from the initial injection area. To increase the number of neutrons detected, and hence obtain good statistics, an array of 20×20 detectors was employed with their counts aggregated. These were arranged over a central 200×200 m area which was found to be sufficient to limit the possibility of an individual detector being influenced by its neighbors (detectors make up only 1% of the central area), while also ensuring that all detectors are many neutron mean-free paths away from the edge of the neutron injection region. The (typically small) error bars on plots of neutron count show the statistical (Poisson) uncertainty due to the finite number, N of detected neutrons and are given by \sqrt{N} . This same uncertainty is translated into an uncertainty in the footprint (Figures 5c and 5d) using the cumulative count curves (e.g., as shown in panel a of the same figure).

Neutron detectors were also simulated at varying displacements, x from a boundary between soil ($x < 0$), and concrete ($x > 0$) to model the experiment described in Section 2.5.1. The Volumetric Water Content (VWC) of the soil was set to 20% to approximately match the mean of 20.7% recorded by TDR measurements in the experiment (Figure 7a). A computationally efficient way to obtain acceptable statistics (a sufficiently high number of detected neutron) is to again use an array of detectors in order to increase the fraction of injected neutrons that get detected. However, in this case only the counts for detectors within the same column of the array (that is, with the same displacement x from the boundary) are aggregated. Because of this, a single simulation employing an $M \times M$ array of detectors generates results for M different displacements, while for each displacement M times greater count are expected compared to a simulation employing a only single detector. The results, presented later (Figure 7d), combine two simulations employing $M = 40$ and $M = 39$, and using a reduced spacing between detectors of 5 m (centered on $x = 0$). This enabled the simulation of detectors for displacements $-97.5 \text{ m} \leq x \leq 97.5 \text{ m}$ in steps of 2.5 m. Results for the outer two columns, $\pm 97.5 \text{ m}$ and $\pm 95 \text{ m}$, were removed to eliminate possible edge effects, and the slight difference in detector numbers between $M = 40$ or $M = 39$ was accounted for. In this case, a total of 400 million neutrons were injected per simulation to obtain adequate statistic.

Apart from where stated, the modeling conducted in this study employs detector elements with the idealized neutron response consisting of 100% efficient detection and absorption over the water-sensitive neutron energy range 10^{-6} –0.01 MeV. This will have a modest quantitative effect on the simulation results, simplifies their interpretation, and also prevents them from being tied to the particular type and arrangement of CRNP used in the experiment. This is additionally important as recent developments in CRNS technologies for environmental monitoring include the use of novel lithium (Raymond, 2019) and boron (Lacy et al., 2011; Weimar et al., 2020) converters, scintillation-based instruments (Stevanato et al., 2019), and possible optimization of the response function using Gadolinium to shield thermal neutron, or by adjusting the moderator thickness (Weimar et al., 2020). A detailed simulation specific to the assemblage of boron trifluoride CRNP used in the experiment is presented in Appendix B to allow general features to be distinguished from those that depend on the particular detector response. The effect this has on simulation results will be noted.

2.4. Field Sampling and Calibration

In our experiments, to measure the SM ground truth, standard field soil sampling procedures were adapted from (Franz, 2012; Zreda et al., 2012). The soil sampling spatial pattern was designed to follow an estimated spatial weighting of the CRNS sensor, to readily facilitate comparison or calibration. Soil samples for volumetric SM and bulk density determination were typically taken from 18 locations centered on the measurement position of the rover: In each of six compass directions (0° , 60° , 120° , 180° , 240° , and 300°) and at each of three distances (1, 2, and 5 m) from the probe. The reduced sampling footprint was designed to provide high spatial resolution SM reference measurements for the case of multiple rover sampling locations, with partially overlapping footprints. In principle, as the rover transects a field, stopping at, for example, 25 m intervals to acquire a SM measurement, reference samples around the new location provide additional

reference measurements at greater distance for the neighboring rover sampling locations. This is true along a single transect, and is achieved normal to the transect by the rover making parallel transects, to complete a raster sampling of the field.

However, where single transects were measured, for calibration of the rover, a 10-m width (5 m either side of the transect) does not fully represent the rover footprint (see Figures 5a and 5b later), and could lead to biases. It is shown later that for the Blankney trial, SM variability at the 300 m scale is quite low; thus, any biases are expected to be small. For the single point airfield calibration, any sampling bias is less important, as the objective was to assess the wet to dry transition. The samples (at 1, 2, and 5 m from the rover) are equally weighted when compared with the CRNS measurements, due to the exponentially declining sensitivity with distance from the CRNP (although this may not properly account for the detailed footprint sensitivity, and future work should use computed sample weightings for the reduced footprint). At each location, samples were taken from five depths covering 0–25 cm below ground level with 5 cm increments; when comparing to the CRNP, these are again given an exponential weighting (Köhli et al., 2015), reducing with distance from the soil surface. This procedure gives a target total of 90 samples. The soil samples are taken using standard 50 mm internal diameter, 51 mm length, sample rings, giving a volume of 100 cm³. Having removed surface vegetation, the rings were inserted in the vertical orientation using a closed ring holder. The samples were transferred to sealed plastic bags and returned to the laboratory for analysis, where the initial mass of each sample is recorded. The samples were oven dried at 105°C for 36 h and the mass recorded again allowing volumetric SM and dry bulk density to be calculated (Gardner, 1986). The CRNP footprint weighted average of all 90 samples is then used as the reference volumetric SM content for calibration. Soil samples for the determination of lattice and bound water and soil organic carbon were taken following the sampling procedure described in (Franz, 2012; Schrön et al., 2017).

2.5. Description of Sites

Two field experiments were conducted. The first objective was to demonstrate changes of the neutron count rate as the rover moved incrementally across a transect from a wet to dry area. The change of neutron counts with distance from the wet/dry boundary was required to assess the footprint length scale of the rover with and without additional moderator. This was tested by traversing the rover along a single line which comprised a field of grass (with relatively high soil water content) and large area of concrete (with very low water content) on a former military airfield. The second experiment was used to demonstrate how the rover could measure SM at high spatial and temporal resolution.

2.5.1. Airfield, Lincolnshire Aviation Heritage Centre, UK

The first experiment was conducted at the Lincolnshire Aviation Heritage Centre (Lincolnshire Aviation Heritage Centre, 2020) located in East Kirkby, Lincolnshire, England (53°08′20.2″N, 0°00′14.5″E). The robot traversed a grass field and a large area (30 ha) of concrete hard standing. The soil type in the grass part is slowly permeable seasonally wet slightly acidic clay loam. The concrete slabs were 30 cm thick with a drainage underneath. The drainage grates were 91.5 cm long and 38 cm wide. The transect was 240 m long, and was made with and without a 5-cm HDPE moderator covering the top and sides of the detectors (not the bottom). Neutron counts were collected for 10 min at 1, 2, 4, 8, 16, 32, 64, and 120 m on both sides from the concrete-grass borderline as shown in Figure 2. TDR measurements were also performed at 1, 2, 4, 8, 16, 32, 64, and 120 m on the grass side immediately following neutron count collection at each point (three TDR measurements from the immediate vicinity – a radius of 20 cm – of each point were averaged). The measurements were performed by a portable TDR using 7.6 cm rod lengths (Model FieldScout TDR150, Spectrum Technologies, Inc.) on February 5 and 6, 2019. The average temperatures and relative humidity for the measurement durations on each day were 3.9°C and 6.7°C and 96% and 86%, respectively.

2.5.2. Stubble Field in Blankney, Lincolnshire, UK

Figure 3 shows the location of the stubble field in Blankney, Lincolnshire, England (53°05′52.5″N, 0°27′37.2″W) used to demonstrate the application of the rover at high spatial and temporal resolution. The soil type of the field is Shallow lime-rich clay loam soil, over limestone. The measurements were performed between 07:00 h BST and 15:00 h BST for three consecutive weeks (on August 1, 8, and 14, 2018) after the field was harvested. All of these measurements used the additional moderator on the rover, and additional



Figure 2. Aerial photograph of Lincolnshire Aviation Heritage Centre. The concrete (dry area) and grass (wet area) parts of the airfield are shown. The measurement points are shown by the dots. The labels show the distance of some of the points from the transect where G and C identify the grass and concrete areas, respectively. The location of the calibration point is 120 m away from the transect into grass area.

point SM measurements were made at each point (A1-F6 in Figure 3-Left) with the portable TDR. No precipitation was reported between the first and second measurements and it was warm and dry; however, before the last measurement there was 32.8 mm precipitation (recorded at nearby RAF Waddington [Met Office, 2018; MIDAS Open: UK Land Surface Stations Data. UK Hourly Rainfall Data, V201908., 2018], on August 9 to 13, 2018, inclusive). As Figure 3 shows an area of 360×360 m was divided into 36 points (a grid of 6×6) with a distance of 60 m between the points. The neutron count was collected at each point for 10 min except for the calibration point for which the neutron counting time was 240 min. On the third measurement day, the neutron count rate was recorded at a reduced number of points due to technical issues.

3. Results and Discussion

3.1. Effect of Additional Moderator

3.1.1. Simulated Reduction of Footprint Due to Additional Moderator

Schematic examples of paths taken by neutrons between their first point of contact with the soil and their eventual detection are shown in Figure 4. Broadly speaking, these paths are divided into two types. Neutrons such as those exemplified by the blue path in Figure 4 are detected almost immediately upon exiting the soil, having only traveled a distance of the order of the detector height (i.e., a few meters). In contrast, those neutrons exemplified by the green and red paths have typically traveled distances of several atmospheric

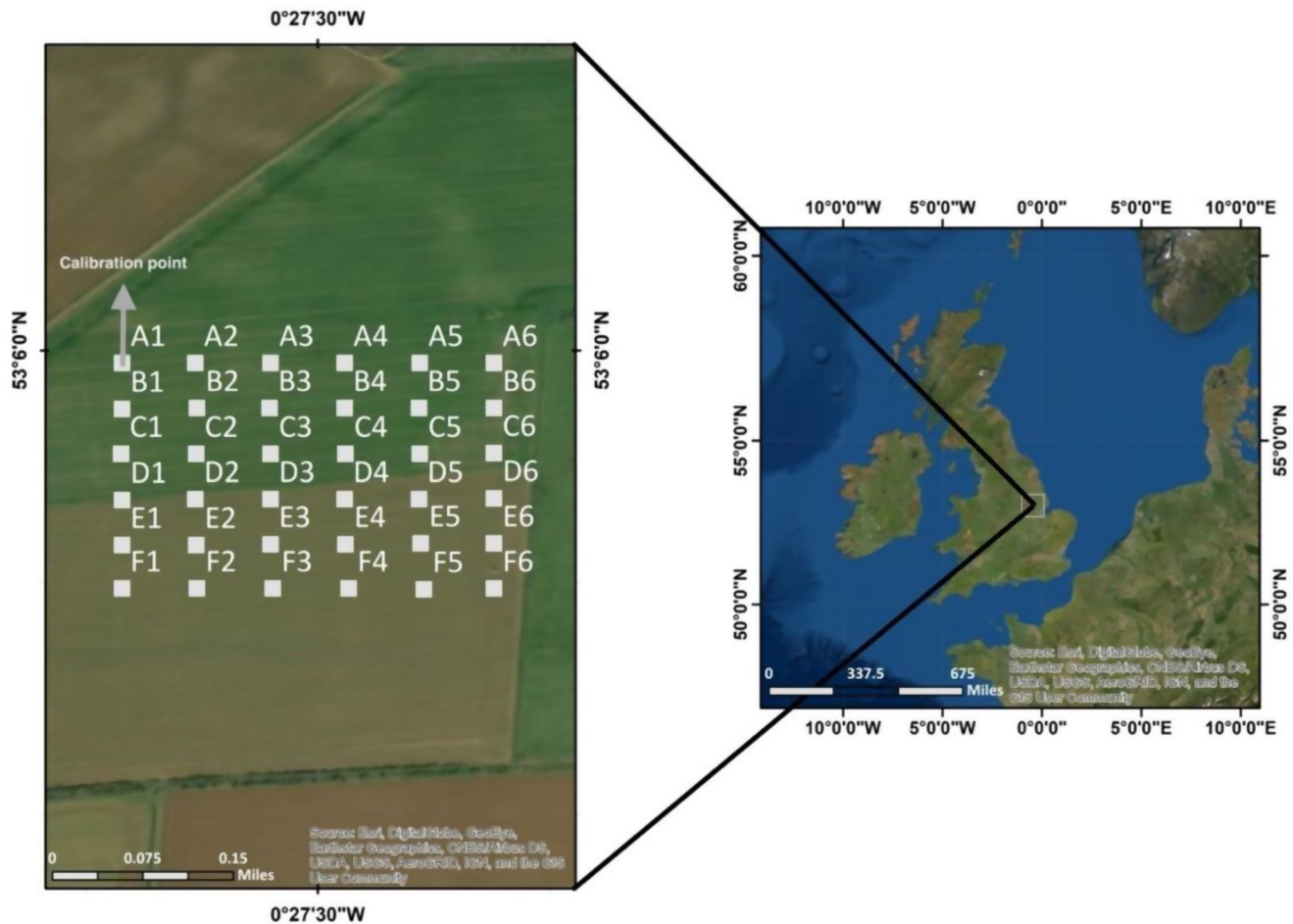


Figure 3. (Left) The Blankney stubble field with sampling points layout (white circles). The distance between the points is 60 m (A1 is the calibration point). (Right) The location of Blankney in the UK.

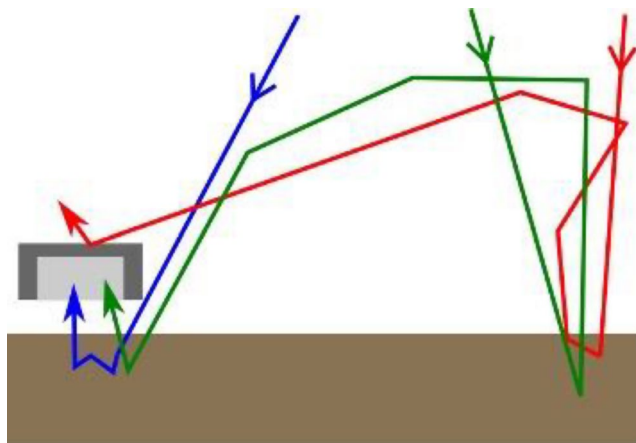


Figure 4. Schematic diagram comparing typical neutron paths that travel either short distances from their first point of contact with soil (blue path), or long distances (red and green paths). The neutron detector is shown in light gray, additional high-density polyethylene moderator is shown in dark gray, and the brown area represents the soil.

mean-free paths (i.e., tens or hundreds of meters) and have possibly had multiple separate interactions with the soil. Adding a moderator to the detector tends to suppress paths of this second type (as they may enter the detector from above), while having a far more limited effect on neutrons entering directly from their first contact with the soil (as these enter the detector from below).

Here, a footprint distance for an individual neutron is defined as the straight line distance between its first point of contact with the soil and its eventual detection in the detector (Köhli et al., 2015). Using the neutron transport code URANOS (Köhli et al., 2015; Köhli, 2019) we produce simulations of the percentage counts detected from within certain footprint distances, for detectors with either 0, 5, or 10 cm of additional HDPE moderator (Figure 5a). In all three cases, there is an initial step increase in counts over the first few meters arising predominantly from neutrons with the first type of path (blue path, Figure 4). This is followed by a much smoother increase persisting over hundreds of meters, arising from neutrons with the second type of path (green and red, Figure 4). Additional moderator suppresses the detection of neutrons with the second type of path, resulting in a considerable increase in the percentage of neutrons with smaller footprint distances. For example, at VWC = 20%,

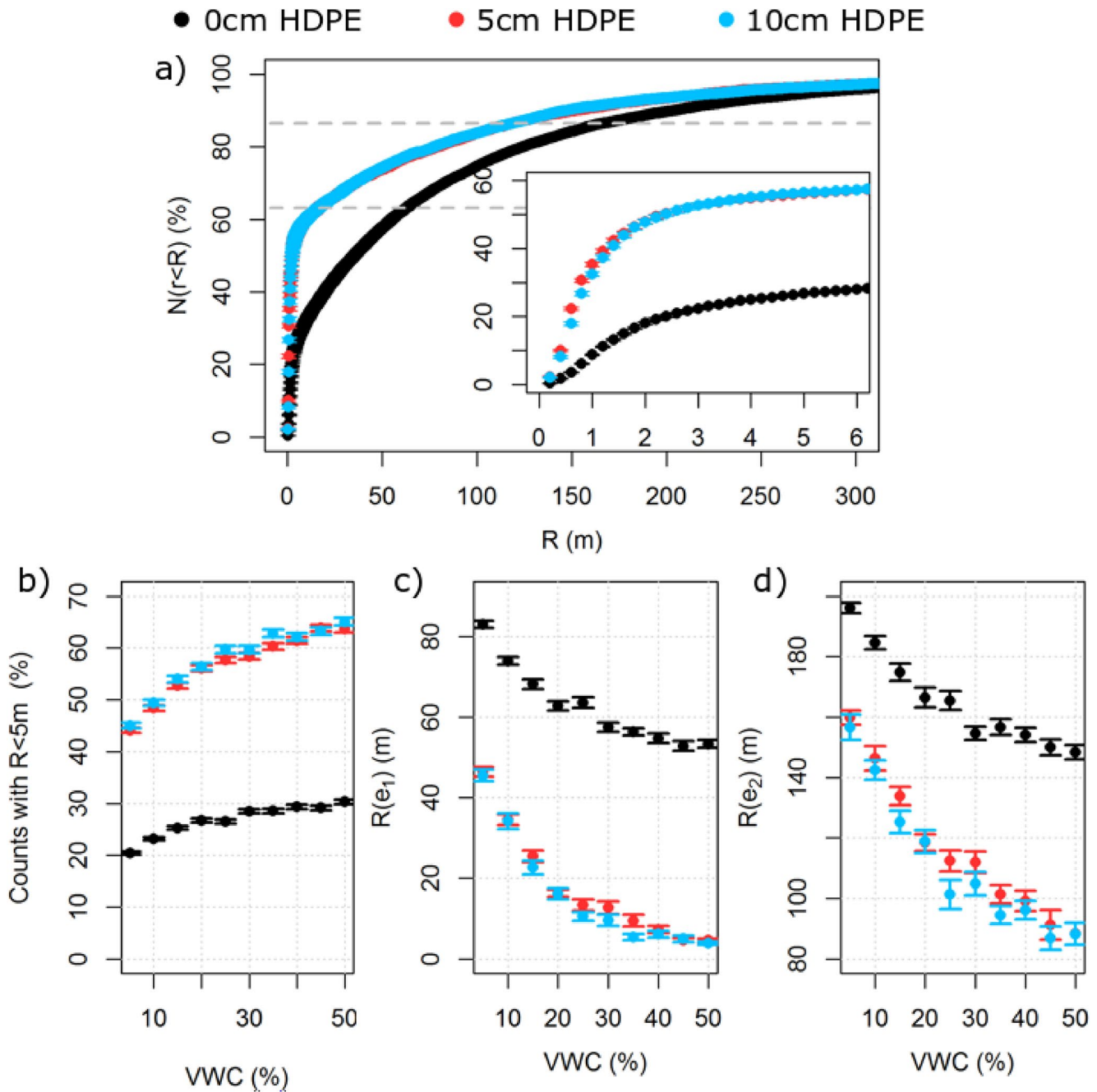


Figure 5. (a) Simulated percentage counts with footprint distances less than R , for Volumetric Water Content (VWC) = 20%. Gray dashed lines mark $e_1 \approx 63\%$ and $e_2 \approx 86\%$. The inset displays a zoom on the first 6 m. (b) The percentage counts with a footprint distance of less than 5 m, (c) The dependence of footprint distance $R(e_1)$ on simulated VWC, (d) The same for $R(e_2)$.

the percentage of counts from within 5 m is approximately doubled from 27% for no additional moderator to 56% for both 5 and 10 cm of additional moderator. Figure 5b shows that the percentage counts detected from within 5 m approximately doubles when HDPE moderator is added for the range of SMs tested.

Conventionally, overall footprint distances of $R(e_1)$ or $R(e_2)$ are defined as the radii such that either $e_1 = 1 - e^{-1} \approx 63\%$ or $e_2 = 1 - e^{-2} \approx 86\%$ of detected neutrons have smaller footprint distances (Desilets & Zreda, 2013; Köhli et al., 2015; Zreda et al., 2008). In Figure 5a, these thresholds are displayed as gray dashed horizontal lines. Previously, simulated $R(e_2)$ footprints were found to depend on the atmospheric

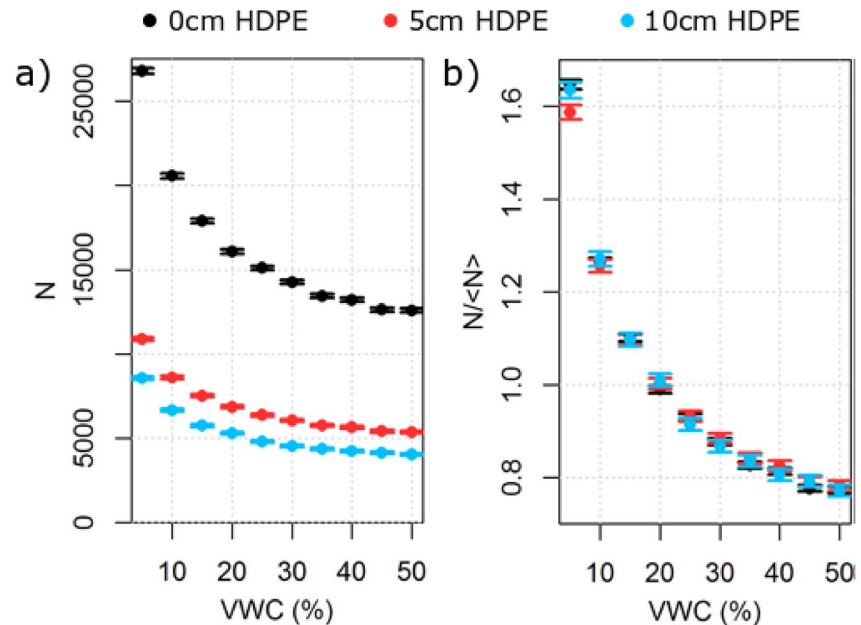


Figure 6. (a) Detected counts as a function of simulated Volumetric Water Content for detectors with varying levels of additional moderator. (b) The same as (a) except that counts have been divided by their mean for each thickness of additional moderator.

humidity in (Desilets & Zreda, 2013), while both $R(e_1)$ and $R(e_2)$ footprints were found to depend on the humidity and the SM in (Köhli et al., 2015).

Figures 5c and 5d display the $R(e_1)$ and $R(e_2)$ footprints of detectors with/without additional moderator at a fixed humidity of 10 g/m^3 . The $R(e_1)$ footprint shows both a strong reduction due to additional moderator as well as a strong dependence on the SM. For example, at $\text{VWC} = 20\%$, the footprint distance $R(e_1) = 62.8 \pm 1.2 \text{ m}$ for a detector without additional moderator is reduced to $R(e_1) = 16.3 \pm 0.9 \text{ m}$ for 5 cm of additional moderator. In contrast, the relative changes to the $R(e_2)$ footprints are more modest. This is expected as the much higher threshold used in the $R(e_2)$ footprint means that it is sensitive to the long-distance tails of the $N(R)$ -distribution (Figure 5a) which are produced by the neutrons such as those exemplified by the green and red paths Figure 4. Later (Section 3.1.3) we will show that the $R(e_1)$ footprint better represents the distance over which changes in SM can be sensed. Nevertheless, using a single distance to represent curves such as Figure 5a is always going to be problematic.

In Figure 5, all curves for 5 and 10 cm of HDPE are very similar suggesting that further increasing the moderator thickness will have a modest additional effect on the sensor's performance. This is further confirmed in Appendix B (Figure B2) where detailed modeling of the rover shows that 5 cm of HDPE is sufficient to block the majority of neutrons, excepting some of those with the highest energies, $E > 0.1 \text{ MeV}$. Alternatively, using response functions in Appendix B to represent a detailed model of the rover with a realistic representation of the specific detectors used in the experiment (rather than the idealized detector response function used to produce Figure 5, see Section 2.3), has a modest (but non-zero) quantitative effect on footprint distances. For example, using $\text{VWC} = 20\%$ results in $R(e_1) = 55.0 \pm 0.8 \text{ m}$ for 0 cm HDPE, or $R(e_1) = 29.1 \pm 0.7 \text{ m}$ for 5 cm HDPE.

3.1.2. Simulated Effect of Additional Moderator on the Soil Moisture Calibration Curve

Converting a measured neutron count rate into a soil VWC requires a calibration curve (i.e., the monotonically decreasing function connecting the two quantities; see Appendix A, Equation A6). Figure 6a displays the neutron counts detected for simulations performed with different SMs. As expected, neutron counts decrease both as VWC is increased, and as additional moderator is added. In Figure 6b, the curves for the

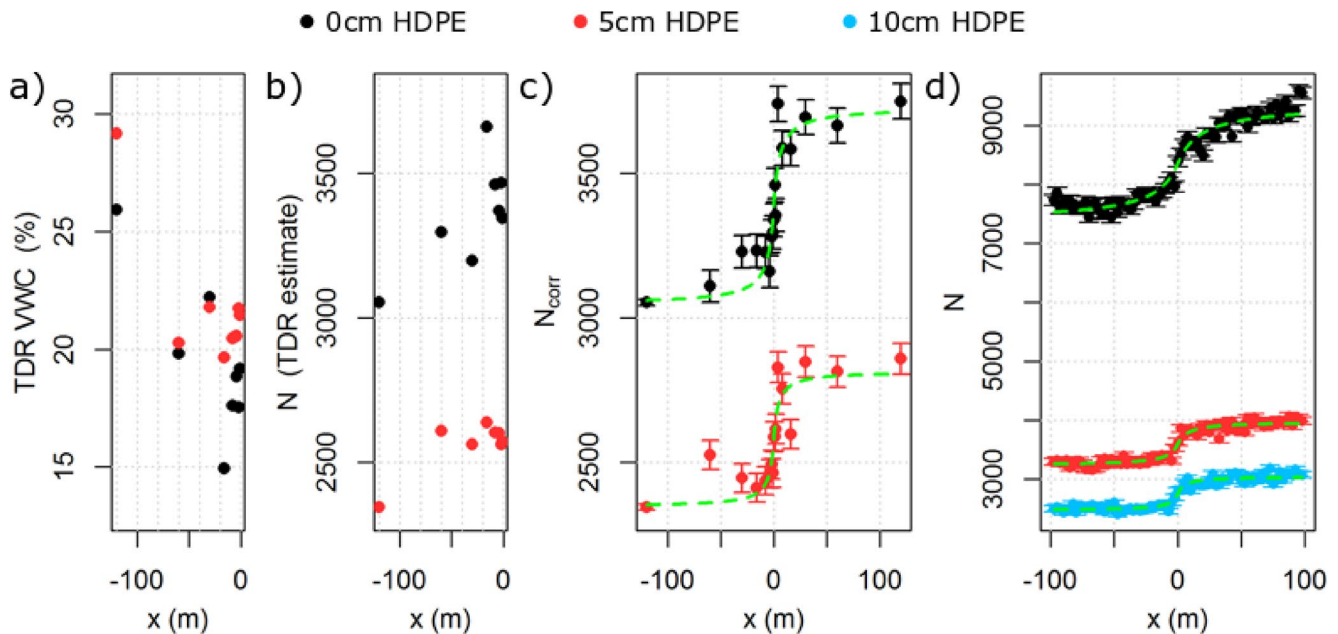


Figure 7. Volumetric Water Content (VWC) and neutron counts across a boundary between soil ($x < 0$) and concrete ($x > 0$). (a) Time domain reflectometry (TDR) VWC measurements for the soil part of the transect performed on the same day and in the same location as the corresponding neutron count measurement show in (c). (b) An estimate of the neutron counts for a uniform soil with a VWC given by the corresponding TDR measurement. (c) Counts measured using the rover. The smaller uncertainty for $x = -120$ m is because of the longer averaging period used for that point. (d) Simulated counts. Dashed green lines in (c) and (d) show the sigmoid curve $n(x)$ (Equation 1 using maximum likelihood estimates for d^* , \bar{N} , and ΔN).

three thicknesses of HDPE moderator have been divided by their mean value. The fact that these curves lie approximately on top of each other demonstrates that the additional moderator only affects the overall scale of the curve without significantly altering its shape.

In practice, the scaling of the curve is taken care of by a parameter (N_0 in Equation A6) which is calibrated using manual soil sampling of VWC from within the detector's footprint. When the additional moderator is added, spatial weighting of the VWC determined from soil samples from different distances from the rover must therefore be adjusted in accordance with the appropriate footprint. A reasonable rule of thumb is to simply double the weighting given to samples within a distance of 5 m from the detector. This reflects that fact that the percentage counts from within this distance approximately doubles for detectors with additional moderator regardless of the SM conditions (Figure 5d).

Tests using the realistic response functions (developed in Appendix B) showed a very limited ($<10\%$) change in the shape of the curve relating neutron counts to VWC (presumably due to differing degrees of water sensitivity at different neutron energies; Weimar et al., 2020), and no additional change in shape when the additional moderator was added. However, the relative reduction of the counts produced by the additional moderator was found to be far more modest than is visible in Figure 6a. This will be discussed further in Section 3.1.3 with reference to the measured neutron counts.

3.1.3. Measured and Simulated Count Rates Across a Soil-Concrete Transect

Figures 7c and 7d compare simulated neutron counts and measured neutron counts (corrected as per Appendix A) at varying displacements along the transect across a boundary between soil ($x < 0$) and concrete ($x > 0$) shown in Figure 2. In both cases, the lower hydrogen content of the concrete results in an increase in the neutron count across the boundary. The length scale over which this change occurs is related to the detector's footprint. Here we extract length scales from the measured/simulated neutron count data in order to (i), show that the footprint distance $R(e_1)$, rather than $R(e_2)$, relates better to the distance over which changes in SM can be sensed, and (ii), to attempt to validate the reduction in footprint distance produced by additional moderator. To determine the length scale for the change in neutron counts, we fit statistical

Table 1
Maximum Likelihood Estimates and 95% Equal Tailed Credible Interval for Length Scale, d

	HDPE	d^*/m	$R(e_1)$ (m)	$R(e_2)$ (m)
Simulation	0 cm	18.2 [13.7, 24.8]	68.2 ± 1.2	174.9 ± 2.9
	5 cm	7.9 [4.7, 13.9]	25.4 ± 1.5	133.9 ± 3.1
	10 cm	5.5 [3.1, 10.0]	22.7 ± 1.7	125.3 ± 3.7
Experiment	0 cm	5.4 [3.0, 13.5]	-	-
	5 cm	4.3 [2.1 15.1]	-	-

Poisson noise is assumed to be the only source of error. Theoretical $R(e_1)$ and $R(e_2)$ footprints for VWC = 15% are also displayed. HDPE, high-density polyethylene.

models to each set of data. In these models, the neutron count, N_i at each displacement, $x = x_i$ is given by a sigmoid function, $n(x_i)$ describing the expected counts, plus a random error,

$$N_i = n(x_i) + \epsilon_i, n(x) = \bar{N} + \Delta N \frac{x/d}{\sqrt[1+\nu]{1 + |x/d|^\nu}} \quad (1)$$

Here, $\bar{N} - \Delta N$ and $\bar{N} + \Delta N$ are the expected counts over soil and concrete, respectively, d is the length scale over which the change occurs, and the exponent $\nu = 1$ was chosen based on its good fit for the simulated data. The error term is taken to be normally distributed $\epsilon_i \sim \mathcal{N}(0, \sigma_i^2)$ with zero mean and the standard deviation $\sigma_i = \sqrt{N_i}$ expected from the statistical (Poisson) error due to the finite numbers of neutrons detected. In reality, ϵ_i will also include errors due to inaccuracies in the choice of $n(x)$, such as those caused by a potentially inaccurate choice of ν , the fact

that the assumed symmetry $n(x) - \bar{N} = \bar{N} - n(-x)$ is only approximately correct, and for the experiment, the effects of SM heterogeneity and so forth.

Using Bayes' rule, the (marginal) probability of d for given set of counts data $\{N_i\}$ is

$$\Pr(d | \{N_i\}) = \frac{1}{\Pr(\{N_i\})} \prod_i f_{\sigma_i}(\epsilon_i) d \bar{N} \Delta N, \quad (2)$$

where $f_{\sigma_i}(\epsilon_i)$ is the probability density function for $\mathcal{N}(0, \sigma_i^2)$, and $\Pr(\{N_i\})$ is the normalization constant. In the experiment, the neutron count for the first measured point ($x = -120$ m) was averaged for a time period of 240 min, compared to just 10 min for the remaining points. This was included in the model by reducing the uncertainty for this point by a factor of $\sqrt{24}$ and is reflected in the reduced size of its error bar in Figure 7c.

Maximum likelihood estimates and 95% credible intervals for d , calculated using Equation 2, are given in Table 1. For the simulated data, increased thicknesses of additional moderator consistently reduce the maximum likelihood estimate, d^* albeit with some overlap of the credible intervals.

Table 1 also provides the simulated $R(e_1)$ and $R(e_2)$ footprint distances for a VWC of 15%, which is the average of the VWC of the simulated soil (20%) and the effective VWC of the concrete (10%). Both the $R(e_1)$ and $R(e_2)$ distances are considerably larger than the corresponding d^* values. However, for the $R(e_1)$ distance, the ratio between the two is fairly small, and is approximately constant: $R(e_1) / d^* = 3.7, 3.2, 4.1$ for an addition of 0, 5, and 10 cm of HDPE moderator, respectively. In contrast, the same ratio for the $R(e_2)$ distance is both considerably larger and non-constant: $R(e_2) / d^* = 9.6, 16.9, 22.8$. This suggests that the $R(e_2)$ footprint distance is not appropriate for understanding the length scale over which variations in the SM can be sensed. Part of the reason that the ratio $R(e_1) / d^*$ is greater than one could be explained by the fact that $R(e_1)$ is more properly compared to the distance $x \approx 1.7d^*$ for which $n(x) / n(0) = e_1$ is obtained. However, there are also differences in the geometries used in the calculation of d^* compared to $R(e_1)$, and the fact that a definition of the footprint distance for an individual neutron is required to calculate $R(e_1)$ which is not the case for d^* .

The d^* values extracted from the experiment are also dramatically smaller than the corresponding theoretical $R(e_2)$ distances, but are also considerably smaller than the theoretical d^* values and do not display a comparable reduction when the additional moderator is installed. Note however that the credible intervals are large, and only account for the statistical (Poisson) noise in the neutron counts, while neglecting the potentially considerable uncertainty due to the deviations from the expected count behavior caused by SM heterogeneity.

Figure 7a displays TDR point measurements of SM from the soil side of the transect – each point shows the average of three measurements performed on the same day and in the vicinity of the corresponding neutron count measurement displayed in Figure 7c. Figure 7b displays an estimate of the neutron counts expected for a homogeneous soil with the corresponding TDR SM, in order to help quantify the effect SM variations might have on the measured neutron counts. The conversion between TDR VWC and estimated neutron count is obtained by scaling the VWC-count data shown in Figure 6 to the measured counts for $x = -120$ m at each level of additional HDPE moderator, and then using a linear interpolation between points. Note this neutron count estimation does not account for the presence of the concrete area, and would therefore be expected to be constant for homogeneous SM.

The uncertainty generated by SM heterogeneity can, approximately, be quantified by the standard deviation of the neutron counts estimates shown in Figure 7b and is given by 184.6 or 91.4 for the estimates corresponding to 0 or 5 cm of additional HDPE, respectively. This can be compared to the mean of the expected statistical Poisson noise (\sqrt{N}) for the same measurement in Figure 6c of only 56.5 or 48.5, respectively. Note, however, that the TDR measurements may exaggerate the SM variation as sensed by the rover (which is averaged over a footprint), and only applies to the soil half of the transect. Nevertheless, this suggests the credibility intervals for the measured d^* values in Table 1 should be extended considerably such that they probably compatible with the values extracted from the simulation (but clearly not enough for them to be compatible with the $R(e_2)$ distances).

In Figure 7, the addition of 5 cm of moderator only reduces the measured neutron count by approximately 24%. This is a far smaller reduction than the 57% found for the simulation, and also far smaller than is expected given the proportion of detector covered by the additional moderator. The reason for this appears to be due to the fact that the neutron detectors used in the experiment are likely to be far less than 100% efficient (Köhli et al., 2018), which contrasts with the perfect neutron detection and absorption employed for the simulated detectors in Figure 7c. When simulations were conducted using the realistic detector response functions developed in Appendix B (VWC = 20% and a 20×20 of detectors were used as per Section 2.3) the addition of 5 cm of moderator only resulted in a 27% reduction in the number of detected neutrons. Alternatively, using an idealized detector response (100% efficient detection for $10^{-6} \text{ MeV} \leq E \leq 0.01 \text{ MeV}$) but setting detectors as 100% transparent (rather than 100% absorbing) so that each neutron is counted but passes through unhindered, resulted in a reduction in the neutron count by only 42% when 5 cm of moderator was added. These results can be explained by the possibility of neutrons scattering off the inside of the additional moderator resulting in multiple chances of detection. Because of this, the reduction in the experimentally measured count rate due to additional moderator is rather modest, conveniently resulting in only a modest increase in statistical noise.

3.2. Measurements From a Stubble Field in Blankney, Lincolnshire, UK

The raw neutron count was corrected for atmospheric pressure variation, atmospheric water vapor variation and incoming neutron flux intensity using Equations A1–A4 in Appendix A and VWC was calculated from N_{corr} via Equations A5 and A6. Figure 8 shows the calculated VWC at the measurement points (Figure 3). Although 10 min of data collection was considerably lower compared to 240 min at the calibration point, the standard deviation values on Figure 8 shows 10 min of neutron counting gives reasonable results and also it is practical in large fields to achieve accurate results in much shorter time. Figure 8 shows an average reduction in VWC of 1.8 percentage points between week 1 and week 2. Measurements made after 32.8 mm of rain in week 3, show there is a significant increase (on average 7.9 percentage points) in the VWC. The TDR readings agree well with the VWC calculated from the neutron counts (indicating that variability is due to real SM changes, rather than some other measurement artifact); although there is a slight discrepancy in week 3 which may be explained by the time required for infiltration of the rainfall. Clearly, a heavy rain event following a long dry period, combined with a relatively slow soil infiltration rate, could lead to the topmost 5 cm of soil being significantly wetter than the 5–10 cm soil depth layer, leading to real differences in the observations by different techniques that have different soil depth sensitivities.

The rover measured VWC is also presented in Figure 9 as measurement dots to show SM spatial variation over three weeks.

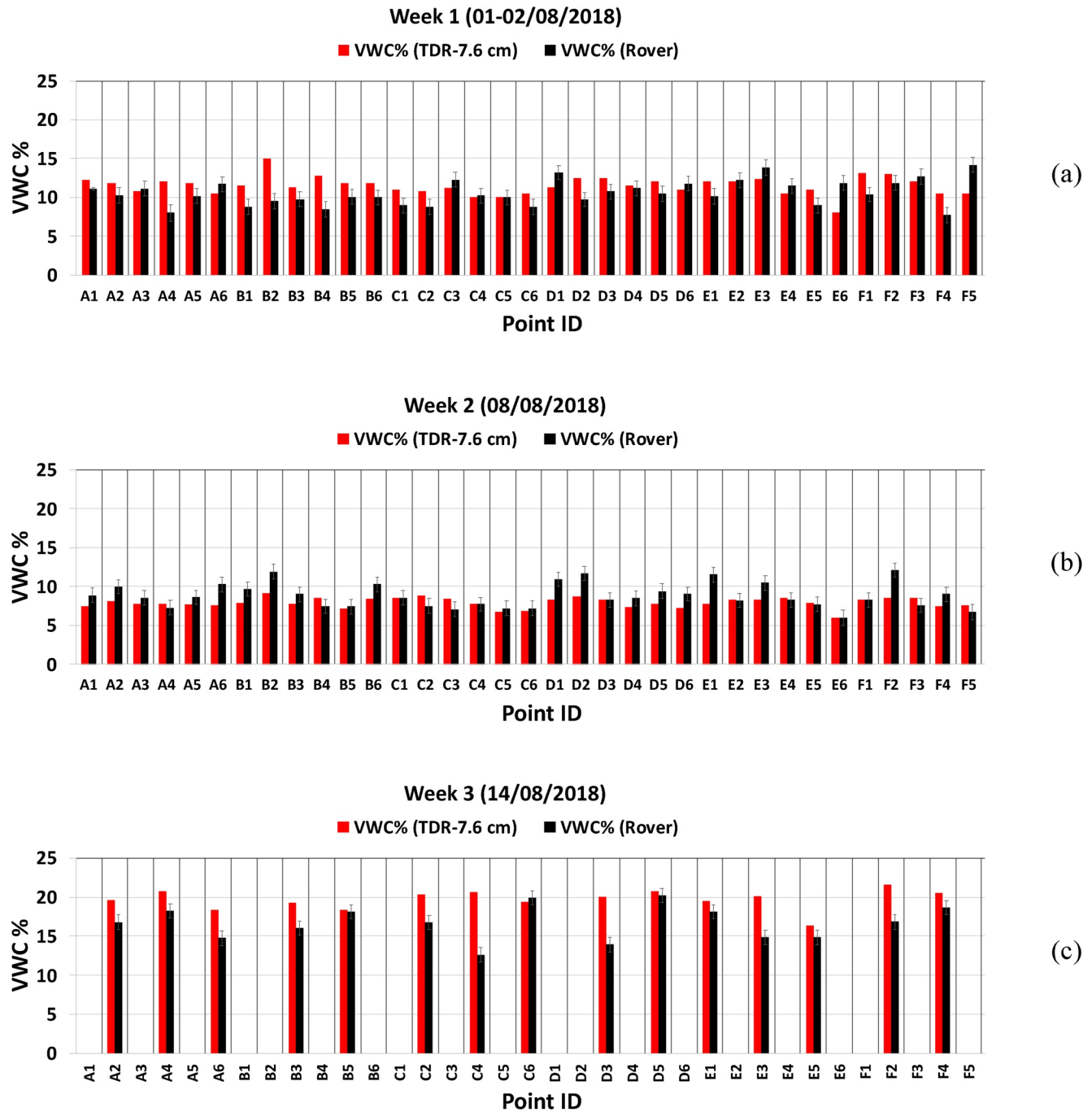


Figure 8. (a) Volumetric Water Content (calculated from neutron count) and time domain reflectometry measurements on (a) 01–02/08/2018, (b) 08/08/2018 and (c) 14/08/2018.

4. Conclusion

This study presents a novel mobile CRNP mounted on a robotic platform, and optionally fitted with additional HDPE moderator on the top and sides of the detectors to modify its footprint. Neutron transport modeling using the Monte Carlo code URANOS, has been used to show that the additional moderator can reduce the footprint effectively. For example, at $VWC = 20\%$ and with atmospheric humidity 10 g/m^3 , the $R(e_1)$ footprint distance was reduced from $62.8 \pm 1.2 \text{ m}$ without additional moderator to $16.3 \pm 0.9 \text{ m}$ by 5 cm

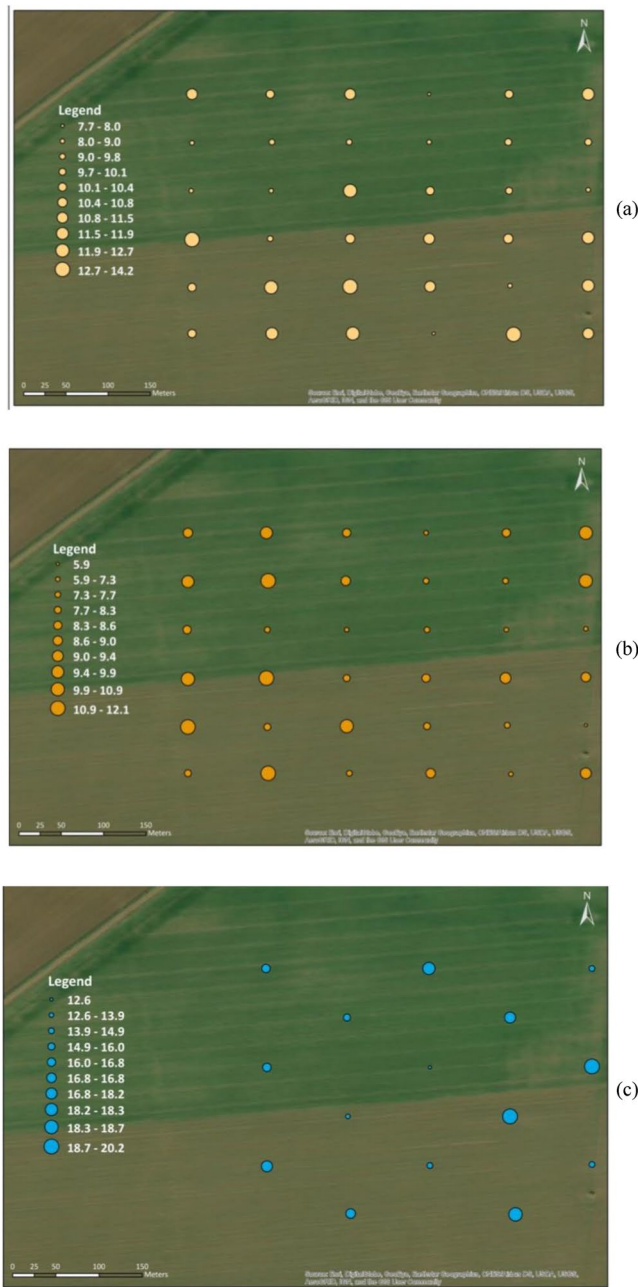


Figure 9. Rover measured soil moisture (Volumetric Water Content% calculated from neutron count) over three weeks. (a) 01–02/08/2018, (b) 08/08/2018, and (c) 14/08/2018 (for reduced number of points). The point labels follow the layout in Figure 3.

of additional moderator. Only modest additional benefit was found if the modeled 5 cm of additional moderator was increased to 10 cm.

Broadly speaking, neutron paths detected by the rover can be divided into two types (Figure 4): Those that typically enter the detector from below having only traveled a few meters from their first point of contact with the soil, and those that may enter from above or below having traveled distances of several atmospheric mean free paths (i.e., tens or hundreds of meters). The additional moderator tends to suppress detection of neutrons of this second type, resulting in approximately a doubling of the percentage of counts detected from within 5 m of the detector.

Simulations and measurements of neutron counts across a transect between areas of grass and concrete were performed. Both showed appreciable changes in the neutron count over length scales of tens of meters, which is much smaller than would be expected from the $R(e_2)$ footprint distance. In the simulation, additional moderator was found to reduce this length scale in proportion to the reduction of the $R(e_1)$ footprint distance. A comparable reduction in length scale was not found with the measured neutron counts due to large uncertainties arising from both statistical (Poisson) noise in the counts and a large SM heterogeneity. Additional moderator was found to only reduce the measured count rate by approximately 24%. This is consistent with detailed modeling (Appendix B) which allows for the multiple scattering of neutrons within the additional moderator, and conveniently means that the increase in the statistical (Poisson) noise is modest. Further modeling revealed that installing additional moderator does not change the shape of the calibration curve linking SM to neutron counts.

The rover with additional moderator was trialed in a stubble field alongside a TDR over three weeks with varying SM, to assess the suitability of the reduced footprint detectors in measuring spatial and temporal SM variations. The potentials of an autonomous mobile SM surveyor have been assessed. However, further research and tests need to be performed in different environmental conditions to prove the capabilities of the mobile surveyor. Such autonomous systems could prove to be competent in agriculture fields especially with further developments in novel solid state neutron detectors.

Further research is still required to fully validate experimentally the footprint sensitivity of detectors with additional moderator, especially with the impact of low vegetation in mind since the detectors are exposed mainly from the bottom. Experimental uncertainty could be reduced with either longer counting intervals, or more sensitive detector banks. More detailed consideration of the full sensor footprint, or testing over very large homogeneous areas, may also lead to closer agreement of modeling versus experiment. The modular non-permanent moderator arrangement also enables further investigation on the orientation and positioning of the moderator and the possibility of integrating such

a moderator on other systems. The impact of the modeling details on neutron counts compared to typical realizations of the detector is also another open area, which requires further research.

Appendix A: Corrections Applied to the Measured Neutron Count

A1. Correcting for Atmospheric Pressure Variation

Neutron counts were corrected for the influence of atmospheric pressure (Evans et al., 2016; Hawdon et al., 2014; Schrön, 2017; Zreda et al., 2012) via Equation A1,

$$F_p = e^{\beta(P-P_0)} \quad (\text{A1})$$

where F_p is the pressure correction factor and β is the barometric pressure coefficient (A value of $\beta = 1/130 \text{ hPa}^{-1}$ was used across all sites, although there is a small dependence on latitude; Zreda et al., 2012). Barometric pressure, P , is measured on site and an arbitrary value of 1,000 hPa is assumed for P_0 .

A2. Correcting for Atmospheric Water Vapor Variation

Neutron counts were corrected for the influence of atmospheric water vapor (Evans et al., 2017; Rosolem et al., 2013; Schrön, 2017; Zreda et al., 2012) through Equation A2,

$$F_h = 1 + 0.0054(h - h_0) \quad (\text{A2})$$

where F_h is the humidity correction factor, h is absolute humidity (gm^{-3}) which is calculated from the site measured temperature and relative humidity. h_0 is the average absolute humidity (gm^{-3}) for the calibration duration.

A3. Correcting for Incoming Neutron Flux Intensity

Neutron counts were corrected (Schrön, 2017) for variations in background intensity based on data collected at Jungfrauoch neutron monitoring station and available from the neutron monitoring database (www.nmdb.eu/), using Equation A3,

$$F_I = I_0 / I \quad (\text{A3})$$

where F_I is the neutron intensity correction factor, I is the count rate at Jungfrauoch monitoring station and I_0 is the count rate at Jungfrauoch monitoring station during the calibration.

A4. Corrected Neutron Counts and Volumetric Water Content

Corrected neutron count (N_{corr}) comes from multiplication of the correction factors and raw neutron count (N_{raw}) by Equation A4,

$$N_{\text{corr}} = N_{\text{raw}} \times F_p \times F_h \times F_I \quad (\text{A4})$$

The corrected neutron counts are totaled up to 10 min of running time for each point then they are converted to Volumetric Water Content (VWC) using,

$$\theta_v = \theta_g \frac{\rho_{bd}}{\rho_w} \quad (\text{A5})$$

and

$$\theta_g = \left(\frac{a_0}{\frac{N_{\text{corr}}}{N_0} - a_1} - a_2 - (\tau + \text{SOC}) \right) \quad (\text{A6})$$

where θ_v and θ_g are the volumetric SM content ($\text{m}^3 \text{m}^{-3}$) and gravimetric SM (g g^{-1}), ρ_{bd} and ρ_w are the dry bulk density and the density of liquid water, respectively. The parameter values a_0 , a_1 , and a_2 are 0.0808, 0.372, and 0.115, respectively (Desilets et al., 2010). τ is the fraction of lattice and bound water (g g^{-1}) and

SOC is the soil organic carbon (g g^{-1}). The SM value from the field calibration data and the corrected neutron count rate are inserted in Equation A6 to find N_0 and then calculate θ_v .

Appendix B: Detailed Modeling of the Rover's Energy Dependent Neutron Response and Its Effect on Modeled Characteristics

Here a detailed model of the rover is developed, including the specific detector assemblage used in the experiment, in order to distinguish those features of the modeling that depend on the particular type and arrangement of detectors from those that don't. These simulations were produced following the method in (Köhli et al., 2018). The rover was modeled using up to 6 layers of voxels, with a horizontal resolution of 5×5 mm, to represent the 12 boron trifluoride proportional counters (stacked as per Figure 1a), the three HDPE moderator containers, any air gaps, and when used, the additional 5 or 10 cm of HDPE moderator on the top and sides of the detector. Energy dependent neutron response functions for the rover as a whole were determined for each side by spline-interpolating the number of neutrons absorbed in the boron trifluoride proportional counters for 41 simulations of mono-energetic neutrons (scaled logarithmically in energy). This allowed a detailed examination of the characteristics of the detector, and also provided a method of accounting for the fine details of the detector in simulations using a coarser horizontal resolution. This part of the work employed version 0.99 ω 13 of URANOS.

Figure B1 shows density distributions of neutron tracks for exemplary horizontal cross sections through detailed models a rover exposed to a neutron flux from above. For thermal neutrons (Figures B1a and B1c), HDPE moderator is clearly visible from its higher track density resulting from its higher material density, while the boron trifluoride proportional counters are visible as a reduced track density due to their absorption of neutrons. In contrast, epithermal and fast neutrons (Figure B1b), are more homogeneously distributed within the casing as their mean-free path is much longer than that of the thermal neutrons. Figure B1c

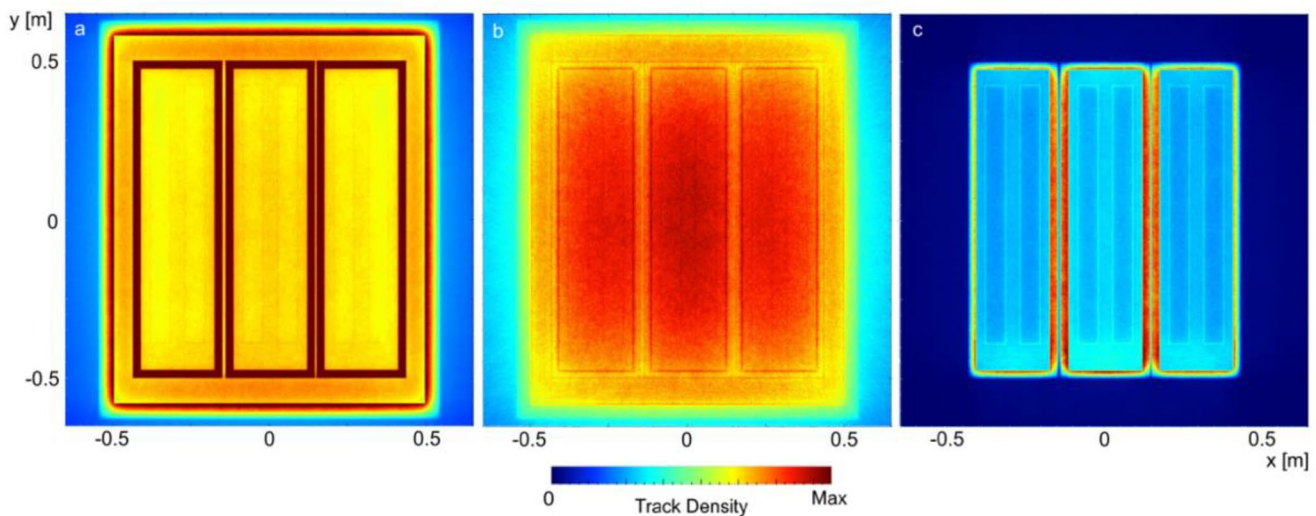


Figure B1. Simulated neutron track densities for a horizontal cross-section through the rover containing the boron trifluoride tubes (contained in three rectangular high-density polyethylene cases). The model is exposed to a homogeneous neutron source flux from the top. (a) Thermal neutron distribution for a rover with 5 cm of additional moderator, (b) epithermal neutron distribution for a rover with 5 cm of additional moderator, (c) the thermal neutron distribution for a rover without additional moderator.

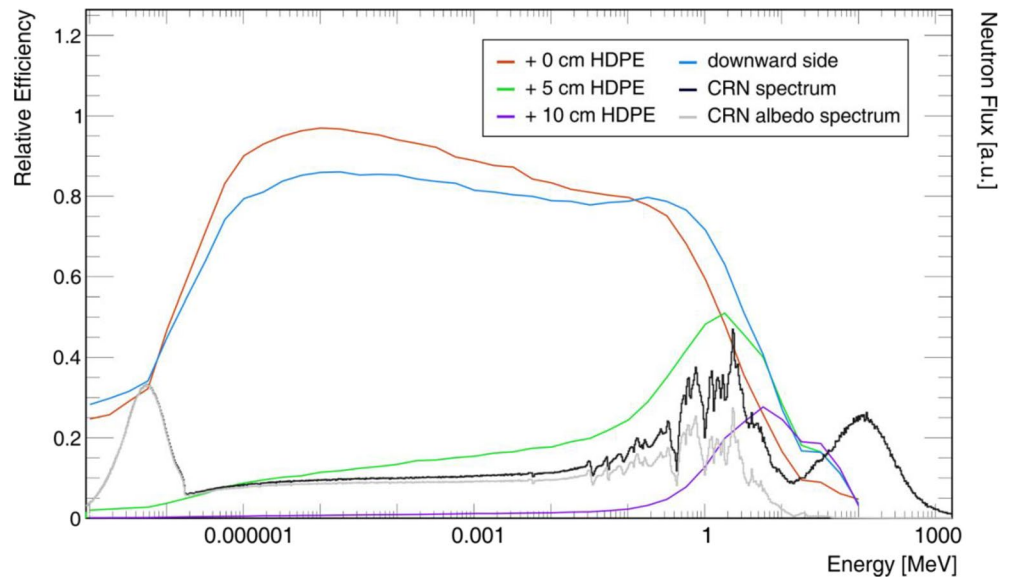


Figure B2. Response function for detailed models of the rover with the indicated thicknesses of additional high-density polyethylene (HDPE) moderator (red, green, and purple lines) for neutrons impinging from the top. The response function for a 5-cm of additional HDPE and neutrons impinging from the bottom is also displayed (blue line). Both directions are equivalent 0 cm HDPE. The cosmic-ray neutron spectrum and the environmental albedo spectrum (i.e., spectra of neutrons that have probed the soil) are also displayed (use right axis).

additionally shows that the neutron track density for the central case of boron trifluoride proportional counters is slightly boosted by the presence of the outer units when the neutron flux comes from above.

The characteristics of the whole rover (HDPE + boron trifluoride + air gaps + optional additional moderator) treated as a single neutron detecting entity are captured in the energy dependent neutron response functions, Figure B2, which provide detection efficiencies for neutrons impinging on the top or bottom of the rover. As expected, use of additional moderator on the top and sides of the rover results in a considerable reduction of the detector efficiency for neutrons impinging on the upper surface. However, even 10 cm of additional moderator is insufficient to fully suppress counts from high-energy neutrons. These are largely formed of incoming radiation and therefore have little sensitivity to soil VWC. The effect of the additional moderator for neutrons impinging on the underside of the detector is less dramatic but still present. Also, note that the additional moderator acts to increase the effective detecting surface area (i.e., the surface area of the rover as a whole).

Data Availability Statement

The MET data are available from the CEDA archive in the Natural Environment Research Council's Data Repository for Atmospheric Science and Earth Observation (<http://archive.ceda.ac.uk/>).

Jungfraujoch neutron monitor data were kindly provided by the Cosmic Ray Group, Physikalisches Institut, University of Bern, Switzerland (<http://www.nmdb.eu/>).

References

- Al-Yaari, A., Wigneron, J.-P., Ducharne, A., Kerr, Y. H., Wagner, W., De Lannoy, G., et al. (2014). Global-scale comparison of passive (SMOS) and active (ASCAT) satellite based microwave soil moisture retrievals with soil moisture simulations (MERRA-Land). *Remote Sensing of Environment*, 152, 614–626. <https://doi.org/10.1016/j.rse.2014.07.013>
- Andreasen, M., Jensen, K. H., Desilets, D., Zreda, M., Bogena, H. R., & Looms, M. C. (2017). Cosmic-ray neutron transport at a forest field site: The sensitivity to various environmental conditions with focus on biomass and canopy interception. *Hydrology and Earth System Sciences*, 21, 1875–1894. <https://doi.org/10.5194/hess211875201710.5194/hess-21-1875-2017>
- Avery, W. A. (2016). *The Cosmic-Ray Neutron Probe method for estimating field scale soil water Content : Advances and applications*.

Acknowledgments

The authors are very grateful to the support of Lincolnshire Aviation Heritage Centre, Mr Philip Panton, Blankney Estate and the landowners of the study sites for their support. The authors would also like to thank Ian Gould, Halvard Grimstad, and Remy Zakaria for their support in data collection. This work was funded by the Science and Technology Facilities Council (STFC) Newton Fund programme, project ID ST/N006836/1.

- Avery, W. A., Franz, T., Wahbi, A., Dercon, G., Heng, L., & Strauss, P. (2018). Mobile soil moisture sensing in high elevations: Applications of the cosmic ray neutron sensor technique in heterogeneous terrain. In *EGU General Assembly 2018* (Vol. 20(6)). (November), EGU2018-9781.
- Baatz, R., Bogen, H. R., Hendricks Franssen, H. J., Huisman, J. A., Montzka, C., & Vereecken, H. (2015). An empirical vegetation correction for soil water content quantification using cosmic ray probes. *Water Resources Research*, *51*(4), 2030–2046. <https://doi.org/10.1002/2014WR016443>
- Baroni, G., & Oswald, S. E. (2015). A scaling approach for the assessment of biomass changes and rainfall interception using cosmic-ray neutron sensing. *Journal of Hydrology*, *525*, 264–276. <https://doi.org/10.1016/j.jhydrol.2015.03.053>
- Beljaars, A. C. M., Viterbo, P., Miller, M. J., & Betts, A. K. (1996). The anomalous rainfall over the United States during July 1993: Sensitivity to land surface parameterization and soil moisture anomalies. *Monthly Weather Review*, *124*(3), 362–383. [https://doi.org/10.1175/1520-0493\(1996\)124<0362:TAROTU>2.0.CO;2](https://doi.org/10.1175/1520-0493(1996)124<0362:TAROTU>2.0.CO;2)
- Bethe, H. A., Korff, S. A., & Placzek, G. (1940). On the interpretation of neutron measurements in cosmic radiation. *Physics Reviews*, *57*(7), 573–587. <https://doi.org/10.1103/PhysRev.57.573>
- Bogen, H. R., Herbst, M., Huisman, J. A., Rosenbaum, U., Weuthen, A., & Vereecken, H. (2010). Potential of wireless sensor networks for measuring soil water content variability. *Vadose Zone Journal*, *9*(4), 1002–1013. <https://doi.org/10.2136/vzj2009.0173>
- Bogen, H. R., Huisman, J. A., Baatz, R., Hendricks Franssen, H.-J., & Vereecken, H. (2013). Accuracy of the cosmic-ray soil water content probe in humid forest ecosystems: The worst case scenario. *Water Resources Research*, *49*(9), 5778–5791. <https://doi.org/10.1002/wrcr.20463>
- Chrisman, B., & Zreda, M. (2013). Quantifying mesoscale soil moisture with the cosmic-ray rover. *Hydrology and Earth System Sciences*, *17*(12), 5097–5108. <https://doi.org/10.5194/hess-17-5097-2013>
- Desilets, D., & Zreda, M. (2013). Footprint diameter for a cosmic-ray soil moisture probe: Theory and Monte Carlo simulations. *Water Resources Research*, *49*(6), 3566–3575. <https://doi.org/10.1002/wrcr.20187>
- Desilets, D., Zreda, M., & Ferré, T. P. A. (2010). Nature's neutron probe: Land surface hydrology at an elusive scale with cosmic rays. *Water Resources Research*, *46*(11). <https://doi.org/10.1029/2009WR008726>
- Dirmeyer, P. A. (1999). Assessing GCM sensitivity to soil wetness using GSWP data. *Journal of the Meteorological Society of Japan*, *77*(1B), 367–385. https://doi.org/10.2151/jmsj1965.77.1B_367
- Dong, J., Ochsner, T. E., Zreda, M., Cosh, M. H., & Zou, C. B. (2014). Calibration and validation of the COSMOS Rover for surface soil moisture measurement. *Vadose Zone Journal*, *13*(4). <https://doi.org/10.2136/vzj2013.08.0148>
- Entekhabi, D., Njoku, E. G., Houser, P., Spencer, M., Doiron, T., Yunjin Kim, Y., et al. (2004). The hydrosphere State (hydros) Satellite mission: An Earth system pathfinder for global mapping of soil moisture and land freeze/thaw. *IEEE Transactions on Geoscience and Remote Sensing*, *42*(10), 2184–2195. <https://doi.org/10.1109/TGRS.2004.834631>
- Entekhabi, D., & Rodriguez-Iturbe, I. (1994). Analytical framework for the characterization of the space-time variability of soil moisture. *Advances in Water Resources*, *17*(1–2), 35–45. [https://doi.org/10.1016/0309-1708\(94\)90022-1](https://doi.org/10.1016/0309-1708(94)90022-1)
- Entin, J. K., Robock, A., Vinnikov, K. Y., Hollinger, S. E., Liu, S., & Namkhai, A. (2000). Temporal and spatial scales of observed soil moisture variations in the extratropics. *Journal of Geophysical Research*, *105*(D9), 11865–11877. <https://doi.org/10.1029/2000JD900051>
- Evans, J. G., Ball, L., Blake, J., Hitt, O., Wright, G., Cooper, H., et al. (2017). *COSMOS-UK: A new field-scale national soil moisture measurement network*.
- Evans, J. G., Ward, H. C., Blake, J. R., Hewitt, E. J., Morrison, R., Fry, M., et al. (2016). Soil water content in southern England derived from a cosmic-ray soil moisture observing system – COSMOS-UK. *Hydrological Processes*, *30*(26), 4987–4999. <https://doi.org/10.1002/hyp.10929>
- Famiglietti, J. S., Devereaux, J. A., Laymon, C. A., Tsegaye, T., Houser, P. R., Jackson, T. J., et al. (1999). Ground-based investigation of soil moisture variability within remote sensing footprints During the Southern Great Plains 1997 (SGP97) Hydrology Experiment. *Water Resources Research*, *35*(6), 1839–1851. <https://doi.org/10.1029/1999WR900047>
- Famiglietti, J. S., Ryu, D., Berg, A. A., Rodell, M., & Jackson, T. J. (2008). Field observations of soil moisture variability across scales. *Water Resources Research*, *44*(1). <https://doi.org/10.1029/2006WR005804>
- Fermi, E., Amaldi, E., D'Agostino, O., Rasetti, F., & Segre, E. (1934). Artificial Radioactivity Produced by Neutron Bombardment. *Proceedings of the Royal Society A: Mathematical, Physical & Engineering Sciences*, *146*(857), 483–500. <https://doi.org/10.1098/rspa.1934.0168>
- Finkenbinder, C. E., Franz, T. E., Gibson, J., Heeren, D. M., & Luck, J. (2019). Integration of hydrogeophysical datasets and empirical orthogonal functions for improved irrigation water management. *Precision Agriculture*, *20*(1), 78–100. <https://doi.org/10.1007/s11119-018-9582-5>
- Franz, T. E. (2012). *Installation and calibration of the cosmic-ray solar moisture probe*.
- Franz, T. E., Wahbi, A., Vreugdenhil, M., Weltin, G., Heng, L., Oismueller, M., et al. (2016). Using cosmic-ray neutron probes to monitor landscape scale soil water content in mixed land use agricultural systems. *Applied and Environmental Soil Science*, *2016*, 1–11. <https://doi.org/10.1155/2016/4323742>
- Franz, T. E., Wang, T., Avery, W., Finkenbinder, C., & Brocca, L. (2015). Combined analysis of soil moisture measurements from roving and fixed cosmic ray neutron probes for multiscale real-time monitoring. *Geophysical Research Letters*, *42*(9), 3389–3396. <https://doi.org/10.1002/2015GL063963>
- Franz, T. E., Zreda, M., Ferré, T. P. A., & Rosolem, R. (2013). An assessment of the effect of horizontal soil moisture heterogeneity on the area-average measurement of cosmic-ray neutrons. *Water Resources Research*, *49*(10), 6450–6458. <https://doi.org/10.1002/wrcr.20530>
- Gardner, W. H. (1986). In A. Klute (Ed.), *Methods of Soil Analysis: Part 1—Physical and Mineralogical Methods* (2nd ed.). Soil Science Society of America, American Society of Agronomy.
- Grimstad, L., & From, P. (2017). The Thorvald II agricultural robotic system. *Robotics*, *6*(4), 24. <https://doi.org/10.3390/robotics6040024>
- Han, X., Franssen, H.-J. H., Rosolem, R., Jin, R., Li, X., & Vereecken, H. (2015). Correction of systematic model forcing bias of CLM using assimilation of cosmic-ray Neutrons and land surface temperature: A study in the Heihe Catchment, China. *Hydrology and Earth System Sciences*, *19*(1), 615–629. <https://doi.org/10.5194/hess-19-615-2015>
- Hawdon, A., McJannet, D., & Wallace, J. (2014). Calibration and correction procedures for cosmic-ray neutron soil moisture probes located across Australia. *Water Resources Research*, *50*(6), 5029–5043. <https://doi.org/10.1002/2013WR015138>
- Hornbuckle, B., Irvin, S., Franz, T., Rosolem, R., & Zweck, C. (2012). The potential of the COSMOS network to be a source of new soil moisture information for SMOS and SMAP. *IEEE International Geoscience and Remote Sensing Symposium*, 1243–1246. <https://doi.org/10.1109/IGARSS.2012.6351317>
- Institute of Hydrology. (1981). *User's handbook for the Institute of Hydrology neutron probe system* (p. 30). Institute of Hydrology.

- Iwema, J., Rosolem, R., Rahman, M., Blyth, E., & Wagener, T. (2017). Land surface model performance using cosmic-ray and point-scale soil moisture measurements for calibration. *Hydrology and Earth System Sciences*, 21(6), 2843–2861. <https://doi.org/10.5194/hess-21-2843-2017>
- Jakobi, J., Huisman, J. A., Schrön, M., Fiedler, J., Brogi, C., Vereecken, H., & Boga, H. R. (2020). Error estimation for soil moisture measurements with cosmic ray neutron sensing and implications for rover surveys. *Frontiers in Water*, 2. <https://doi.org/10.3389/frwa.2020.00010>
- Jakobi, J., Huisman, J. A., Vereecken, H., Diekkrüger, B., & Boga, H. R. (2018). Cosmic ray neutron sensing for simultaneous soil water content and biomass quantification in drought conditions. *Water Resources Research*, 54(10), 7383–7402. <https://doi.org/10.1029/2018WR022692>
- Kodama, M., Kudo, S., & Kosuge, T. (1985). Application of atmospheric neutrons to soil moisture measurement. *Soil Science*, 140(4), 237–242. <https://doi.org/10.1097/00010694-198510000-00001>
- Köhli, M. (2019). *The CASCADE10B thermal neutron detector and soil moisture sensing by cosmic-ray neutrons*. Heidelberg University. <https://doi.org/10.11588/heidok.00026969>
- Köhli, M., Schrön, M., & Schmidt, U. (2018). Response functions for detectors in cosmic ray neutron sensing. *Nuclear Instruments and Methods in Physics Research Section A: Accelerators, Spectrometers, Detectors and Associated Equipment*, 902, 184–189. <https://doi.org/10.1016/j.nima.2018.06.052>
- Köhli, M., Schrön, M., Zreda, M., Schmidt, U., Dietrich, P., & Zacharias, S. (2015). Footprint characteristics revised for field-scale soil moisture monitoring with cosmic-ray neutrons. *Water Resources Research*, 51(7), 5772–5790. <https://doi.org/10.1002/2015WR017169>
- Koster, R. D. (2004). Regions of strong coupling between soil moisture and precipitation. *Science*, 305(5687), 1138–1140. <https://doi.org/10.1126/science.1100217>
- Lacy, J. L., Athanasiades, A., Sun, L., Martin, C. S., Lyons, T. D., Foss, M. A., & B. Haygood, H. (2011). Boron-coated straws as a replacement for ³He-based neutron detectors. *Nuclear Instruments and Methods in Physics Research Section A: Accelerators, Spectrometers, Detectors and Associated Equipment*, 652(1), 359–363. <https://doi.org/10.1016/j.nima.2010.09.011>
- Larson, K. M., Small, E. E., Gutmann, E. D., Bilich, A. L., Braun, J. J., & Zavorotny, V. U. (2008). Use of GPS receivers as a soil moisture network for water cycle studies. *Geophysical Research Letters*, 35(24), 1–5. <https://doi.org/10.1029/2008GL036013>
- Li, D., Schrön, M., Köhli, M., Boga, H., Weimar, J., Jiménez Bello, M. A., et al. (2019). Can Drip irrigation be scheduled with cosmic-ray neutron sensing? *Vadose Zone Journal*, 18(1), 190053. <https://doi.org/10.2136/vzj2019.05.0053>
- Lincolnshire Aviation Heritage Centre. (2020). <https://www.lincaviation.co.uk>
- McJannet, D., Franz, T., Hawdon, A., Boadle, D., Baker, B., Almeida, A., et al. (2014). Field testing of the universal calibration function for determination of soil moisture with cosmic-ray neutrons. *Water Resources Research*, 50(6), 5235–5248. <https://doi.org/10.1002/2014WR015513>
- McJannet, D., Hawdon, A., Baker, B., Renzullo, L., & Searle, R. (2017). Multiscale soil moisture estimates using static and roving cosmic-ray soil moisture sensors. *Hydrology and Earth System Sciences*, 21(12), 6049–6067. <https://doi.org/10.5194/hess-21-6049-2017>
- Met Office. (2018). *MIDAS open: UK land surface stations data. UK hourly rainfall data, v201908*. http://thredds/fileServer/badc/ukmo-midas-open/data/uk-hourly-rain-obs/dataset-version-201908/lincolnshire/00384_waddington/qc-version-1/midas-open_uk-hourly-rain-obs_dv-201908_lincolnshire_00384_waddington_qcv-1_2018.csv
- Motef, J. (1970). *Neutron fluence measurements*.
- Njoku, E. G., & Entekhabi, D. (1996). Passive microwave remote sensing of soil moisture. *Journal of Hydrology*, 184(1–2), 101–129. [https://doi.org/10.1016/0022-1694\(95\)02970-2](https://doi.org/10.1016/0022-1694(95)02970-2)
- Ochsner, T. E., Cosh, M. H., Cuenca, R. H., Dorigo, W. A., Draper, C. S., Hagimoto, Y., et al. (2013). State of the art in large-scale soil moisture monitoring. *Soil Science Society of America Journal*, 77(6), 1888–1919. <https://doi.org/10.2136/sssaj2013.03.0093>
- Peterson, A. M., Helgason, W. D., & Ireson, A. M. (2016). Estimating field-scale root zone soil moisture using the cosmic-ray neutron probe. *Hydrology and Earth System Sciences*, 20(4), 1373–1385. <https://doi.org/10.5194/hess-20-1373-2016>
- Raymond, A., Inglis, A., & Zreda, M. (2019). Advances in CRNS with lithium-based neutron detectors. *Geophysical Research Abstracts*, 21.
- Robinson, D. A., Campbell, C. S., Hoppmans, J. W., Hornbuckle, B. K., Jones, S. B., Knight, R., et al. (2008). Soil moisture measurement for ecological and hydrological watershed-scale observatories: A review. *Vadose Zone Journal*, 7(1), 358–389. <https://doi.org/10.2136/vzj2007.0143>
- Robinson, D. A., Schaap, M., Jones, S. B., Friedman, S. P., & Gardner, C. M. K. (2003). Considerations for improving the accuracy of permittivity measurement using time domain reflectometry. *Soil Science Society of America Journal*, 67(1), 62. <https://doi.org/10.2136/sssaj2003.6200>
- Rosolem, R., Shuttleworth, W. J., Zreda, M., Franz, T. E., Zeng, X., & Kurc, S. A. (2013). The effect of atmospheric water vapor on neutron count in the cosmic-ray soil moisture observing system. *Journal of Hydrometeorology*, 14(5), 1659–1671. <https://doi.org/10.1175/JHM-D-12-0120.1>
- Saga Robotics. (2020). <https://sagarobotics.com>
- Sato, T. (2016). Analytical model for estimating the zenith angle dependence of terrestrial cosmic ray fluxes. *PloS One*, 11(8), e0160390. <https://doi.org/10.1371/journal.pone.0160390>
- Schrön, M. (2017). *Cosmic-ray neutron sensing and its applications to soil and land surface Hydrology*. Institutional Repository of the University of Potsdam.
- Schrön, M., Köhli, M., Scheffele, L., Iwema, J., Boga, H. R., Lv, L., et al. (2017). Improving calibration and validation of cosmic-ray neutron sensors in the light of spatial sensitivity. *Hydrology and Earth System Sciences*, 21(10), 5009–5030. <https://doi.org/10.5194/hess-215009201710.5194/hess-21-5009-2017>
- Schrön, M., Rosolem, R., Köhli, M., Piussi, L., Schröter, I., Iwema, J., et al. (2018). Cosmic-ray neutron rover surveys of field soil moisture and the influence of roads. *Water Resources Research*, 54(9), 6441–6459. <https://doi.org/10.1029/2017WR021719>
- Schrön, M., Zacharias, S., Köhli, M., Weimar, J., & Dietrich, P. (2015). *Monitoring environmental water with ground PoS (ICRC2015) 231* (pp. 1–7).
- Steele-Dunne, S. C., Rutten, M. M., Krzeminska, D. M., Hausner, M., Tyler, S. W., Selker, J., et al. (2010). Feasibility of soil moisture estimation using passive distributed temperature sensing. *Water Resources Research*, 46(3), 1–12. <https://doi.org/10.1029/2009WR008272>
- Stevanato, L., Baroni, G., Cohen, Y., Fontana, C. L., Gatto, S., Lunardon, M., et al. (2019). A novel cosmic-ray neutron sensor for soil moisture estimation over large areas. *Agriculture*, 9(9), 202. <https://doi.org/10.3390/agriculture9090202>
- Tian, Z., Li, Z., Liu, G., Li, B., & Ren, T. (2016). Soil water content determination with cosmic-ray neutron sensor: Correcting aboveground hydrogen effects with thermal/fast neutron ratio. *Journal of Hydrology*, 540, 923–933. <https://doi.org/10.1016/j.jhydrol.2016.07.004>

- Vather, T., Everson, C. S., & Franz, T. E. (2020). The applicability of the cosmic ray neutron sensor to simultaneously monitor soil water content and biomass in an *Acacia mearnsii* Forest. *Hydrology*, 7(3), 48. <https://doi.org/10.3390/hydrology7030048>
- Wang, A., Zeng, X., Shen, S. S. P., Zeng, Q.-C., & Dickinson, R. E. (2006). Time scales of land surface hydrology. *Journal of Hydrometeorology*, 7(5), 868–879. <https://doi.org/10.1175/JHM527.1>
- Weimar, J., Köhli, M., Budach, C., & Schmidt, U. (2020). Large-scale boron-lined neutron detection systems as a ³He alternative for cosmic ray neutron sensing. *Frontiers in Water*, 2. <https://doi.org/10.3389/frwa.2020.00016>
- Western, A. W., & Blöschl, G. (1999). On the spatial scaling of soil moisture. *Journal of Hydrology*, 217(3–4), 203–224. [https://doi.org/10.1016/S0022-1694\(98\)00232-7](https://doi.org/10.1016/S0022-1694(98)00232-7)
- Western, A. W., Grayson, R. B., & Blöschl, G. (2002). Scaling of Soil Moisture: A Hydrologic Perspective. *Annual Review of Earth and Planetary Sciences*, 30(1), 149–180. <https://doi.org/10.1146/annurev.earth.30.091201.140434>
- Zhu, X., Shao, M. a., Zeng, C., Jia, X., Huang, L., Zhang, Y., & Zhu, J. (2016). Application of cosmic-ray neutron sensing to monitor soil water content in an alpine meadow ecosystem on the northern Tibetan Plateau. *Journal of Hydrology*, 536, 247–254. <https://doi.org/10.1016/j.jhydrol.2016.02.038>
- Zreda, M., Desilets, D., Ferré, T. P. A., & Scott, R. L. (2008). Measuring soil moisture content non-invasively at intermediate spatial scale using cosmic-ray neutrons. *Geophysical Research Letters*, 35(21), 1–5. <https://doi.org/10.1029/2008GL035655>
- Zreda, M., Shuttleworth, W. J., Zeng, X., Zweck, C., Desilets, D., Franz, T., & Rosolem, R. (2012). Sciences COSMOS: The COsmic-ray soil moisture observing system. *Hydrology and Earth System Sciences*, 16, 4079–4099. <https://doi.org/10.5194/hess164079201210.5194/hess-16-4079-2012>